Mean-square amplitudes of vibration and thermodynamic functions of the (0001) surface of graphite

B. Firey, F. W. de Wette, and E. de Rouffignac*
Department of Physics, University of Texas, Austin, Texas 78712

G. P. Alldredge
Department of Physics, University of Missouri—Columbia, Columbia, Missouri 65211
(Received 25 February 1983)

Following our earlier work [Phys. Rev. B 23, 4208 (1981)] on the dynamics of the graphite (001) free surface, we present here the surface and bulk mean-square amplitudes (MSA's) of vibration and the surface thermodynamic functions of graphite. For crystals of finite size, the MSA's depend on the aspect ratio (lateral dimension divided by thickness) and for a given aspect ratio, on thickness. This is of importance for measurements on actual graphite crystals. In addition, this parametrization enables us to carry out an extrapolation to the thermodynamic limit (vanishing surface-to-volume ratio) in a single parameter, namely inverse thickness. For infinitely thick crystals the MSA's are independent of aspect ratio. The surface thermodynamic functions are similar to—but roughly a factor of 10 smaller than—those of more isotropic crystals. This is a result of the weak interplanar binding in graphite which makes the creation of a surface less of a perturbation on the bulk. We find no evidence of a significant contribution from the so-called "flexural mode" in the slab dynamics nor in the surface specific heat.

I. INTRODUCTION

In two recent papers[1,2] (to be henceforth referred to as I and II) we treated the lattice dynamics of a bare graphite slab and of a xenon-covered graphite slab, respectively. The work was motivated by the increasing experimental and theoretical interest in a variety of properties of gases physisorbed on graphite surfaces, but also by the intrinsic interest of changes in the thermodynamic properties caused by the large surface areas and the anisotropy of the "bare" materials. For instance, measurements of heat capacities of a variety of graphite samples by different authors[3–6] have revealed discrepancies for which a number of explanations have been offered (cf. I).

In the present paper we continue our study of the bare graphite (0001) surface by presenting results for the mean-square amplitudes (MSA) of vibration and the surface thermodynamic functions; the calculations were based on the model and methods of the dynamical calculations of I. We present in Sec. II the formulation and, in Sec. III, the results for the MSA's (III A) and for the surface thermodynamic quantities (III B).

II. FORMULATION

Our method of calculation is similar to that described in previous studies of MSA's and thermodynamic functions of noble-gas crystals[7,8] and ionic crystals.[9,10] The first step is to calculate the normal modes of vibration of a graphite slab having two free surfaces parallel to the (0001)-oriented graphite planes and containing N_3 lattice planes; two-dimensional (2D) periodic boundary conditions parallel to the surfaces are applied. The slab unit cell extends through the entire thickness of the slab, and the slab itself is generated by all possible translations of this unit cell parallel to the (0001) planes.

The frequencies $\omega_p(\bar{q})$ and (orthonormalized) eigenvectors $\xi_\alpha(l_3,\kappa;\bar{q},p)$ at a given 2D wave vector $\bar{q}$ are determined by the dynamical matrix equation.

$$\sum_{l_3',\kappa,\beta} D_{\alpha\beta}(l_3,\kappa;l_3',\kappa';\bar{q})\xi_\beta(l_3',\kappa';\bar{q},p)=\omega_p^2(\bar{q})\xi_\alpha(l_3,\kappa;\bar{q},p) , \tag{1}$$

where α,β label the Cartesian coordinates, l_3 is the label of each of the N_3 lattice planes, κ labels the atoms in the 2D unit cell for each plane, and p is the polarization index. The construction of the dynamical matrix and the method of solution have been described in I.

Given the frequencies and eigenvectors, the MSA's and the vibrational thermodynamic functions for the slab are calculated from standard expressions. We have for the MSA's[9]

$$\langle u_\alpha^2(l_3,\kappa)\rangle=(\hbar/2\bar{N}M_\kappa)\sum_{\bar{q},p}{}' \,|\,\xi_\alpha(l_3,\kappa;\bar{q}p)\,|^2 \times\coth[\hbar\omega_p(\bar{q})/2k_BT]/\omega_p(\bar{q}) . \tag{2}$$

The expressions for the internal energy, Helmholtz free energy, entropy, and constant-volume heat capacity are, respectively,[10]

$$E=k_BT\sum_{\bar{q},p}\{\tfrac{1}{2}x+[x/(e^x-1)]\} , \tag{3a}$$

$$F=k_BT\sum_{\bar{q},p}[\tfrac{1}{2}x+\ln(1-e^{-x})]\ , \tag{3b}$$

$$S=k_B\sum_{\bar{q},p}\{[x/(e^x-1)]-\ln(1-e^{-x})\}\ , \tag{3c}$$

$$C_v=k_B\sum_{\bar{q},p}[\tfrac{1}{2}x/\sinh(\tfrac{1}{2}x)]^2\ , \tag{3d}$$

where

$$x=\hbar\omega_p(\bar{q})/k_BT\ . \tag{4}$$

The frequencies used in Eqs. (2) and (3) were obtained from dynamical calculations in which the carbon-carbon force constants were derived from pairwise interactions as given by a modified version of the "axially symmetric" model of Nicklow *et al.*[11] for bulk graphite. The model is described in I, and comparisons with more recent bulk interaction models are made in Ref. 12. (Some errors in the interaction constants in I have been corrected in Ref. 12.)

In the dynamical calculations no corrections have been made for the effects of surface relaxation or for bulk and surface thermal expansion and other anharmonic effects. Let u be any one of the thermodynamic functions reduced to unit quantity of material (per mole or per molecule, say) for the sample having surface area per quantity (n moles or molecules) A/n, and let u^b be the same function for a reference bulk sample having negligible surface area (say, from periodic boundary conditions). We may term the difference

$$\Delta u=u-u^b\ , \tag{5}$$

the surface-excess u, just as is done for experimental determinations of surface thermodynamics. If the surface-excess u is indeed proportional to the relative surface area A/n of the sample, then the surface-specific u defined as

$$U^s=\frac{\Delta u}{A/n}\ , \tag{6}$$

has meaning. Thus we may discuss the surface-specific heat (capacity) C_v^s, the surface(-specific) (internal) energy E^s, the surface(-specific) Helmholtz free energy F^s, and the surface(-specific) entropy S^s, where parenthetical portions of the terms are usually dropped by convention.

III. RESULTS

A. Mean-square amplitudes of vibration

We are interested in calculating mean-square amplitudes for two rather different sorts of systems: first, for the bulk and surface of macroscopically large crystals—i.e., systems for which the surface-to-volume ratio is vanishingly small, and are thus essentially in the thermodynamic limit—and also for the finite and rather small systems which are encountered in typical specimens of graphite and which are subject to significant finite-size effects.

For the first case, in particular, some care is required. If we attempt to compute the MSA's using (2) and a uniformly spaced—i.e., Born—von Kármán—grid of $\bar{q}$ points, we are actually calculating the MSA's for a *finite* sample of graphite, with periodic boundary conditions in the x-y directions and free surfaces in the z direction. An attempt to use a finer grid corresponds to enlarging the sample in the x and y directions, and as is well known[13] will lead to logarithmically divergent MSA's. In order to obtain the true, convergent values of the MSA's appropriate to the three-dimensional (3D) thermodynamic limit, we must use a somewhat more complicated procedure. At this point it is useful to state briefly, first, how we expect the MSA's to behave as functions of slab thickness and slab size, second, what behavior is actually found, and finally, what this means for comparison between calculation and experiment.

1. *Expected behavior of MSA's*

If one considers a slab of fixed edge length and allows the thickness to increase ($N_3\to\infty$), one is effectively computing the MSA's for a one-dimensional system, and they will diverge as N_3. If, on the other hand, one fixes the thickness (N_3 fixed) and increases the edge length, the MSA's will diverge as the logarithm of the edge length (in accordance with the above-mentioned theorem). Instead of specifying a slab by its edge length and thickness, we can specify it by its aspect ratio—defined as the ratio of edge length to thickness—and thickness. In view of what has just been said about the dependence of the MSA's on crystal sizes (thickness and edge length) one is justified in expecting the MSA's for finite crystals of given thickness, say, to be different for different aspect ratios. One is further tempted to expect, albeit without rigorous justification, that if one constructs successively larger slabs of given aspect ratio, then both the bulk and surface MSA's will converge to some finite values.

In fact, the first expectation is found to be true: For a given thickness the MSA's increase with increasing aspect ratio. Furthermore, as we let the crystal grow towards infinite size, the MSA's do indeed converge—moreover, the limiting values are the same for all aspect ratios, for both the bulk and the surface MSA's. This reassuring result, however, may not be of practical importance since most exfoliated graphites on which actual measurements are performed are of rather small thickness, so that the size effects are indeed important. We will come back to these points below.

2. *Details of the calculaton*

The aspect ratio is arrived at in the following way. We adopt an enlarged 2D unit cell, which is suitable for the description of adsorbate properties later on [see Fig. 1(a)]. It has side $a=3a_0$, where $a_0=1.4210$ Å is the inplanar nearest-neighbor (NN) distance between the carbon atoms. We let $d=c/2=3.3539$ Å denote the interplanar distance in graphite. The calculations have been carried out for a lozenge-shaped crystal similar to the unit cell, with side length A and thickness C ($=N_3d$) [see Fig. 1(b)]. The *aspect ratio* is defined as $A/C=\alpha(a/d)$. Calculations have been carried out for three aspect ratios corresponding to $\alpha=1$, 8, and 80 (called cube, slab, and sheet, respectively), and for each aspect ratio for four finite thicknesses

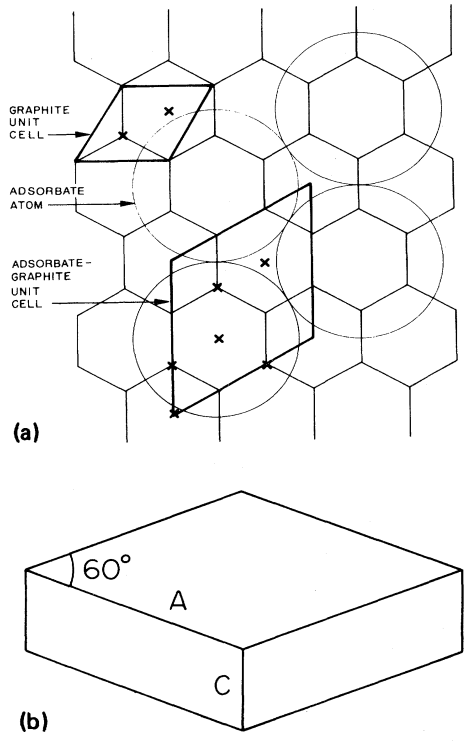

FIG. 1. (a) Krypton or xenon epitaxially adsorbed on the graphite (0001) surface in a $(30°\ \sqrt{3}\times\sqrt{3})$ overlayer structure. Vertices of the hexagonal net mark carbon atoms in the first graphite plane, $\times$ marks carbon atoms in the second graphite plane. (b) Lozenge-shaped crystal with side length A and thickness C.

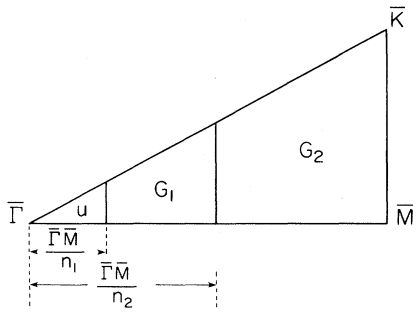

FIG. 2. Division of the ISBZ in parts in which different grids are used. U indicates a uniform grid determined by the lateral size of the crystal and the periodic boundary conditions. G_1 and G_2 indicate Gauss-Legendre quadrature grids. The characteristics of the grids are given in Table I.

$N_3=7$, 13, 21, and 27 as well as their extrapolation to infinite thickness. The reason for this particular procedure—fixed aspect ratio and increasing thickness—is that it is the proper way to approach the thermodynamic limit, i.e., the limit of vanishing surface-to-volume ratio. Because for fixed aspect ratio the surface-to-volume ratio is C^{-1} $[=(N_3 d)^{-1}]$, taking the limit $N_3\to\infty$ is equivalent to taking the thermodynamic limit. The periodic boundary conditions, applied to the sample crystal, determine the density of the wave-vector grid in the (2D) surface Brillouin zone (SBZ).

For a given aspect ratio and thickness one calculates $\langle u_\alpha^2(l_3,\kappa)\rangle$ [Eq. (2)] by summing appropriately weighted contributions from $\bar{q}$ points on this uniform grid in the irreducible part of the SBZ (ISBZ). In practice, however, this method leads to far too many sampling points (e.g., roughly 3900 points for a 27-layer slab). One deals with this problem by observing that the finite resolution of the grid is important only in parts of the ISBZ where the contribution to the MSA is varying rapidly, i.e., near the zone center where the low frequencies occur. Accordingly, one divides the ISBZ into two or three parts—an inner part around the origin in which a uniform grid is used, and one or two outer parts for which the contributions to the MSA's are much less sensitive to the details of the grid. For the latter parts, optimum results are obtained by sampling with much coarser Gauss-Legendre quadrature grids (see the Appendix). The division of the ISBZ is indicated in Fig. 2, and the details of the sampling grids are summarized in Table I.

For a given temperature, one expects the MSA's to converge if one increases the size of the crystal to infinity, while maintaining a fixed aspect ratio. Furthermore, using the layer number N_3 as a measure of the size of the crystal, it is reasonable to expect that the MSA's admit of a series expansion asymptotically valid in $1/N_3$. When the calculations are performed, both expectations are found to be true. Furthermore, for each T the MSA's for the cube, slab, and sheet all approach the same limit for infinite size crystal $(N_3\to\infty)$.

This fact may be understood by considering the related case of the bulk-adapted slab—i.e., a slab in which period-

TABLE I. Characteristics of sampling grids used in various parts of the ISBZ for the evaluation of the MSA's. (Cf. Fig. 2.) G_1 and G_2 indicate the number of points in the Gauss-Legendre grids. $n_1=n_2=1$ means that the entire zone is covered with the uniform grid corresponding to the crystal size. $n_2=1$ $(n_1\neq 1)$ means that the zone is divided into two parts.

Aspect ratio	1				8				80			
N_3	n_1	n_2	G_1	G_2	n_1	n_2	G_1	G_2	n_1	n_2	G_1	G_2
7	1	1			8	1	64		80	8	36	64
13	1	1			8	1	64		80	8	36	64
21	3	1	36		24	1	64		240	24	36	64
27	3	1	36		24	1	64		240	24	36	64

ic boundary conditions are imposed at the top and bottom, rather than the free-surface boundary conditions of the present calculations. In this case, our procedure for calculating the MSA's for a given thickness and aspect ratio corresponds to computing an approximation to the MSA's *of the bulk* with a quadrature rule of the midpoint-rule type; the 3D Brillouin zone is divided into identical prismatic elements, and the integral is approximated by the product of the volume of one element and the sum of the values of the function at the midpoints of the elements—the contribution from the acoustic modes at Γ being excluded. In this case, the aspect ratio determines the shape of the elements, and the thickness the total number thereof; the fact that the extrapolated values are the same simply means that the approximations actually converge to a well-defined integral, despite the singularity in the acoustic contributions—this confirms that the bulk MSA's are well defined.

In the case we actually calculate, with free-surface boundary conditions, the details of the convergence are somewhat less clear. In particular, it is not evident *a priori* that the *surface* MSA's will be well-defined in the same sense as the bulk MSA's. Our results suggest, however, that the essential features are similar; it is thus not surprising that the extrapolated amplitudes are essentially independent of aspect ratio. The fact that this result appears in our numerical calculatons is compelling evidence that our extrapolation procedure leads to the correct MSA's.

If we thus view the amplitudes for slabs of finite thickness as approximations to the true, convergent, values for a semiinfinite piece of graphite, we observe that the errors in the approximations are of varying signs: For the perpendicular components, the finite-slab values are consistently larger than the true ones, while in the parallel case the finite-slab values are consistently smaller. Clearly the sign of the error depends on the details of the functional form of the integrand; we suspect that the difference between the parallel and perpendicular cases involves the anisotropy of graphite.

3. *Results for the MSA's*

As mentioned above, we evaluated MSA's for crystals of three aspect ratios (cube, slab, sheet) and each of these for four thicknesses. The calculations proceed with first solving the equations of motion [Eq. (1)] for the particular sampling grids chosen (Table I) and using the resulting frequencies and polarization vectors to evaluate the MSA's as functions of temperature [Eq. (2)]. The computations were carried out on the Control Data Corporation Cyber 170/750 computer of the University of Texas at Austin. Computational requirements varied from 15 sec of central processing unit (CPU) time [and 10 ft of tape at 6250 CPI (characters per inch) to store the data] for the 7-layer cube to 27 min CPU time (and 1135 ft of tape) for the 27-layer sheet; 80% of the computation time was spent diagonalizing the equations of motion.

The data obtained in this way are too voluminous to present here, and our choice of what to present has been guided by anticipated usefulness. For example, a widely

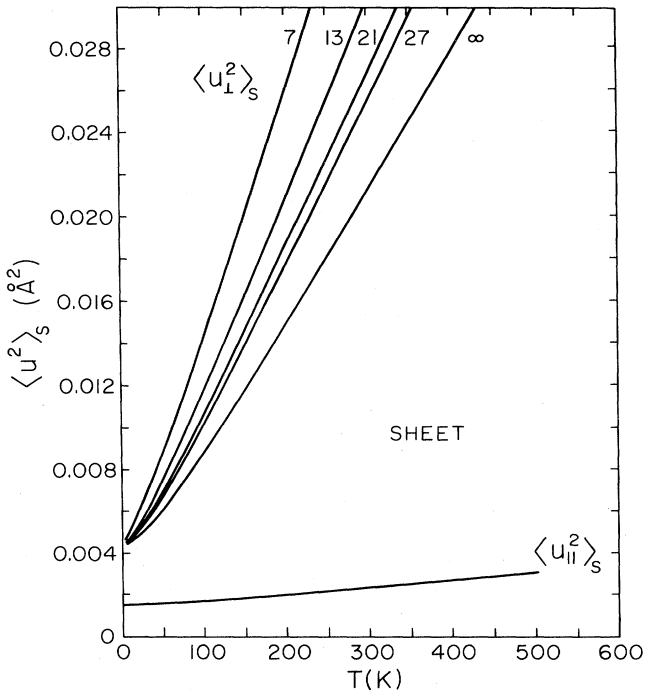

FIG. 3. Surface mean-square amplitudes (MSA) for the 7-, 13-, 21-, and 27-layer sheets and the infinitely thick sheet as functions of temperature. $\langle u_\perp^2 \rangle_S$ indicates the MSA's for the vibrations perpendicular to the surface $\langle u_\parallel^2 \rangle_S$ for the vibrations parallel to the surface. The latter coincides within the thickness of the curve for all sheet thicknesses.

used substrate for adsorption studies is Grafoil.[14] It consists of grains of single crystalline graphite which have large and quite uniform surfaces parallel to the (0001) graphite planes; the lateral extent is of the order of 10^6–10^5 Å. From the width of neutron-scattering Bragg peaks one estimates a coherence thickness of about 100 Å.[15]

In view of these experimental parameters, it appeared most useful to present the MSA data for the sheets. The thickest of these, the 27-layer sheet, has a thickness of 90.6 Å and an edge length of 9208 Å; this is in the range of the actual dimensions of graphite crystallites in Grafoil.

In Fig. 3 we show the MSA's of the surface atoms of the 7-, 13-, 21-, and 27-layer and infinitely thick sheets for vibrations perpendicular and parallel to the surface ($\langle u_\perp^2 \rangle_S$ and $\langle u_\parallel^2 \rangle_S$, respectively). It will be noted that $\langle u_\perp^2 \rangle$ is strongly dependent on thickness, decreasing as the thickness increases and converging to the infinite-thickness value as N_3^{-1}, i.e., proportionally with the vanishing surface-to-volume ratio as pointed out above. This is a finite-size effect; for the smaller thickness, the surface-to-volume ratio is larger, and the entire system is more strongly perturbed by the surface. The effect is not connected with the Landau-Peierls divergence, since it is of opposite sign: At fixed aspect ratio the lateral extent of the system is smaller for the smaller thickness.

It seems almost redundant to point out here that the thickness dependence of the MSA's is an effect that can

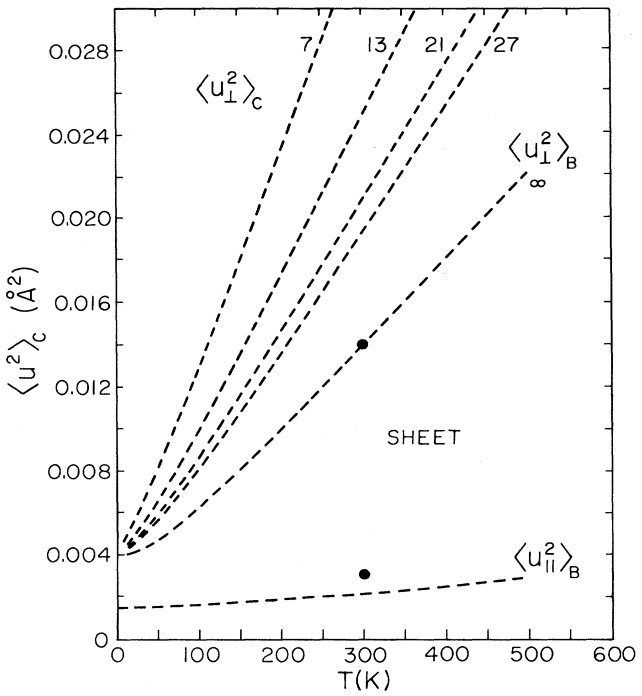

FIG. 4. Center-layer MSA's for the sheets of various thicknesses as functions of temperature. $\langle u_\perp^2 \rangle_C$ for the infinitely thick sheet is the true bulk value $\langle u_\perp^2 \rangle_B$. For the parallel vibrations the center layer MSA's for all sheet thicknesses coincide within the thickness of the line with the bulk value $\langle u_\parallel^2 \rangle_B$. The solid circles at 300 K are the results reported by Chen and Trucano (Ref 18).

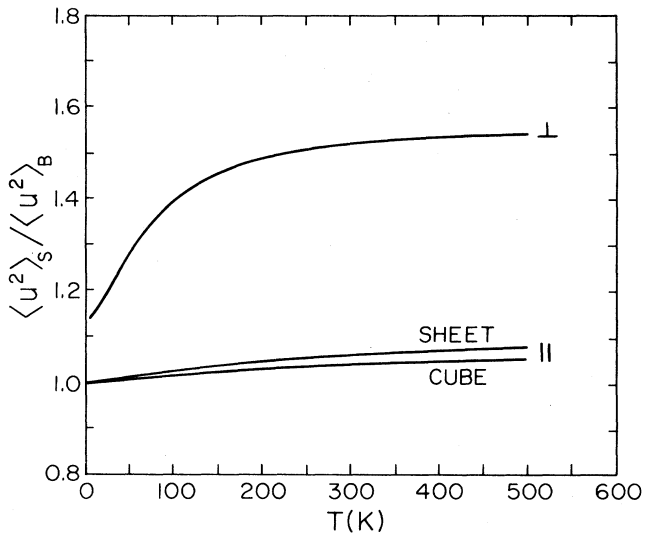

FIG. 5. Temperature variation of the surface MSA enhancement $\langle u^2 \rangle_S / \langle u^2 \rangle_B$ for the infinitely large crystals. For the perpendicular vibrations the curves for the various crystal shapes coincide within the thickness of the line.

only be obtained by calculations on crystals of finite thickness. However, this is important to keep in mind, if one considers alternative methods for calculating surface dynamical properties, such as the matching method, the Green-function method or the continued-fraction method. These methods, as usually applied, all give results that apply to half-infinite crystals and the question of crystal shape (aspect ratio) is not addressed. Fortunately, as we find here, the shape dependence of the MSA's disappears for infinite crystals; but, of course, size effects are not treated by these methods when applied to semiinfinite samples.

In Fig. 4 we show the MSA's for atoms in the center layers of the 7-, 13-, 21-, and 27-layer and infinitely thick sheets, for vibrations perpendicular and parallel to the surface ($\langle u_\perp^2 \rangle_C$ and $\langle u_\parallel^2 \rangle_C$, respectively). The thickness dependence of $\langle u_\perp^2 \rangle_C$ is even more pronounced than that of $\langle u_\perp^2 \rangle_S$. In the limit for an infinitely large crystal $\langle u_\perp^2 \rangle_C$ and $\langle u_\parallel^2 \rangle_C$ approach to the true bulk values $\langle u_\perp^2 \rangle_B$ and $\langle u_\parallel^2 \rangle_B$, and again these bulk values are shape independent; i.e., they are the same for the cube, slab, and sheet.

Finally, in Fig. 5 we show the surface enhancement of the MSA's, which is defined as $\langle u^2 \rangle_S / \langle u^2 \rangle_B$. Since $\langle u^2 \rangle_B$ is defined only for the infinitely large crystals, we only show the curves for that case. Notice that there is a small visible variation in $\langle u_\parallel^2 \rangle_S / \langle u_\parallel^2 \rangle_B$ going from the cube to the sheet; the corresponding variation in $\langle u_\perp^2 \rangle_S / \langle u_\perp^2 \rangle_B$ falls within the thickness of the line.

It is interesting to compare these enhancement results with those of the more isotropic ionic crystals, which we evaluated a number of years ago.[9] It turns out that the surface enhancements for vibrations perpendicular to the surface (z direction) are comparable to those for the ionic crystals, but in contrast to the latter, the in-plane vibrations (x,y directions) show no surface enhancements at $T=0$ K and very little at higher temperatures. This can be attributed to the great strength of the intraplanar interactions compared to the very weak interplanar interactions, which results in a very weak interplanar coupling for the (x, y) vibrations; the absence of one of its neighboring planes hardly alters the (x,y) vibrations in the surface plane.

It is often customary [especially in low-energy electron diffraction (LEED) experiments] to express measured MSA's in terms of Debye temperatures Θ. The reason for this practice is probably that one can express in *one number* the MSA's as a function of temperature, provided the Debye approximation is valid. If this is not the case (and *a priori*, there is no reason to assume that it is) one has to specify the function $\Theta(T)$, and so there is no gain over specifying the MSA's themselves as functions of temperature, except that in a plot of $\Theta(T)$ the deviation from Debye-type behavior becomes very visible; for a Debye system $\Theta(T)$ is a constant. At each temperature the value of $\Theta(T)$ is obtained from $\langle u^2 \rangle_\perp$ be determining the value of Θ which satisfies the relation

$$\langle u_\perp^2 \rangle = \frac{3\hbar^2}{k_B M \Theta} \left[\frac{1}{4} + \frac{\phi(x)}{x} \right], \tag{7}$$

where

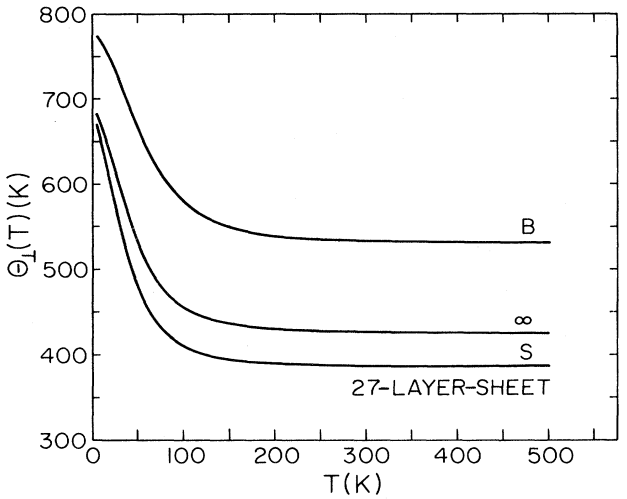

FIG. 6. Debye temperatures $\Theta_\perp(T)$ associated with the perpendicular vibrations for the bulk (B) and for the surface (S), the latter for the infinitely thick crystal and the 27-layer sheet.

$$x=\frac{\Theta}{T}$$

and

$$\phi(x)=\frac{1}{x}\int_0^x \frac{t\,dt}{e^t-1}\ . \tag{8}$$

This exercise is made convenient by using a rational approximation for the Debye function $\phi(x)$.[16]

In Fig. 6 we have plotted the temperature-dependent Debye temperature $\Theta_\perp(T)$ [as obtained from Eq. (7)] for the vibrations perpendicular to the (0001) planes, for the bulk, and for the 27-layer and infinitely thick sheets. The values for $T=5$ and 500 K (the smallest and largest T for which the Θ's have been calculated) are given in Table II. We see a strong temperature variation in $\Theta_\perp(T)$ below 200 K, which indicates a breakdown of the Debye approximation at those temperatures. In Fig. 7 we have plotted the Debye temperatures $\Theta_{||}(T)$ for vibrations parallel to the (0001) planes, for the bulk and the surface. The curves for all cases (cube, slab, sheet; 27 layers and infinitely thick) coincide within the thickness of the line. Because the parallel vibrations are associated with much higher Debye temperatures, there is deviation from Debye-type behavior in the entire temperature range displayed here.

TABLE II. Equivalent Debye temperature $\Theta(T)$ for perpendicular and in-plane vibrations at $T=5$ K and $T\to\infty$ for the bulk and the 27-layer and infinitely thick sheets.

Temperature		5 K	500 K
		$\Theta_\perp$ (K)	
Bulk		774	530
Surface	27-layer sheet	670	385
	thick sheet	681	424
		$\Theta_{||}$ (K)	
Bulk		2046	1653
Surface		2045	1578

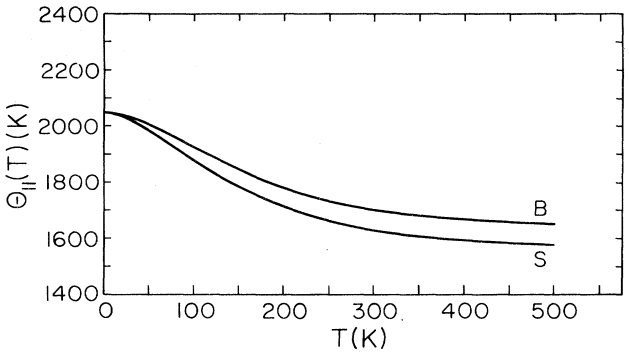

FIG. 7. Debye temperatures $\Theta_{||}(T)$ associated with the in-plane vibrations for the bulk (B) and the surface (S).

4. *Comparison with experiment*

Comparison of the MSA data with experiment is difficult because of the paucity of experimental data, and it is further complicated by numerous uncertainties in unfolding the data to get an MSA. The first mention of bulk MSA's is by Bacon[17] in connection with x-ray diffraction measurements on graphite powder. He quotes a value for $\Theta_\perp^B$ of 560 K (which agrees nicely with our calculated value of 530 K), derived from two reflections, but settles on a mean value of 700 K derived from a series of measurements on a third reflection. Recently, bulk MSA values from x-ray measurements at 300 K on small single crystals were given by Chen and Trucano[18]; the experimental points are indicated in Fig. 4. Notice the excellent agreement of $\langle u_\perp^2\rangle_B$ with our calculation. The agreement for $\langle u_{||}^2\rangle_B$ is not quite as good; we have no explanation for this discrepancy.

The first reported measured surface MSA's that we are aware of were derived from LEED measurements by Albinet *et al.*[19] The authors determined the MSA's on the basis of the temperature variation of the specular spot; in the absence of a full LEED theory, they chose the result for 70-meV electrons, namely $\Theta_\perp=690\pm70$ K, as representative for the surface MSA's. This is substantially higher than our high-temperature value of $\Theta_\perp=424$ K for the infinitely thick crystal. The companion calculations by these authors, based on a first-neighbor (in-plane and out-of-plane) interaction model led to even higher Debye temperatures, i.e., lower MSA's. In this connection we point out that a first-neighbor interplanar interaction model does not provide for coupling between the parallel and perpendicular vibrations and fails to give rise to the Rayleigh surface mode,[1] whose low vibrations make a substantial contribution to the MSA's. In a following paper, which is based on the same interaction model, Biberian *et al.*,[20] calculate the MSA's in the low- and high-temperature limits and compare their results with the Debye approximation, based on the high-temperature Debye temperature. As in Ref. 19 the MSA's come out substantially lower than our results, of course, for the same

reasons. The authors note that the Debye approximation is not valid in the range 0—200 K for $\langle u_\perp^2 \rangle$ and 0—400 K for $\langle u_\parallel^2 \rangle$; our results agree with that observation, for these are precisely the temperature ranges where we find a strong temperature dependence in the corresponding Debye temperatures.

The most recent experimental determination of surface MSA's of graphite was carried out by Boato *et al.*[21] with He-atom scattering. Since the He atoms do not penetrate the surface, one in principle measures true surface phenomena, but the unfolding of the experimental results to obtain surface MSA's necessitates the calculation of the elastic diffraction probability of the specularly reflected beam, which rests on the hard corrugated wall model and on an assumed attractive well interaction. The results for $\langle u_\perp^2 \rangle_S$ agree at 300 K with Chen and Trucano's bulk value and are thus much lower than our calculated results. With the attendant difficulties in arriving at MSA values it is difficult to pinpoint the cause of the discrepancy between these experimenal results and our calculated values. However, the agreement of the He scattering surface results with Chen and Trucano's x-ray bulk results indicates that the MSA's derived from He scattering are too low. Further, Ref. 21 attributes the deviation of the MSA's from Debye behavior to the high anisotropy of graphite. Such a conclusion needs to be substantiated because it is well known that deviations from Debye behavior per se occur for all substances; after all, the Debye spectrum deviates significantly from actual vibrational spectra. For instance, for solid noble gases (which are fairly representative of isotropic materials) the specific-heat Debye temperature for the bulk drops by 15% between $T/\Theta=0$ and 0.1 (Ref. 22); for ionic crystals this variation ranges from 7% (RbCl) to 14% (MgO) (cf. Ref. 10). A similarly pronounced deviation from Debye behavior is not found for the MSA Debye temperatures, however. For instance, for argon we find that the bulk-MSA Debye temperature varies between 83.7 K at $T=0$ K and 84.9 K at $T=50$ K, while the surface-MSA Debye temperature $\Theta_\perp$ for the (111) surface varies between 57.0 and 58.6 K in this same temperature range. In comparison with these minute changes, the variations in graphite are huge. For instance, for the bulk, $\Theta_\perp^B$ and $\Theta_\parallel^B$ vary by 34% and 20%, respectively, between 0 and 500 K, while for the infinitely thick sheet, the variations for $\Theta_\perp^S$ and $\Theta_\parallel^S$ are 38% and 23%, respectively. Without investigating these differences in detail it is somewhat speculative to attribute the large-T variation of a quantity like $\Theta_\perp$ totally to the anisotropy of the lattice (after all, $\Theta_\perp$ applies only to the perpendicular vibrations). It may well be that the close Debye-type behavior of the MSA's of the solid noble gases is in a sense accidental, so that in comparing graphite and solid noble gases, we are comparing two extremes.

B. Surface thermodynamic functions

The surface thermodynamic functions E^S, F^S, S^S, and C_V^S have been evaluated according to Eq. (5). There exists no divergent behavior of these quantities as functions of lateral extent or thickness of the slabs and thus no particular care has to be exercised in the choice of the wave-

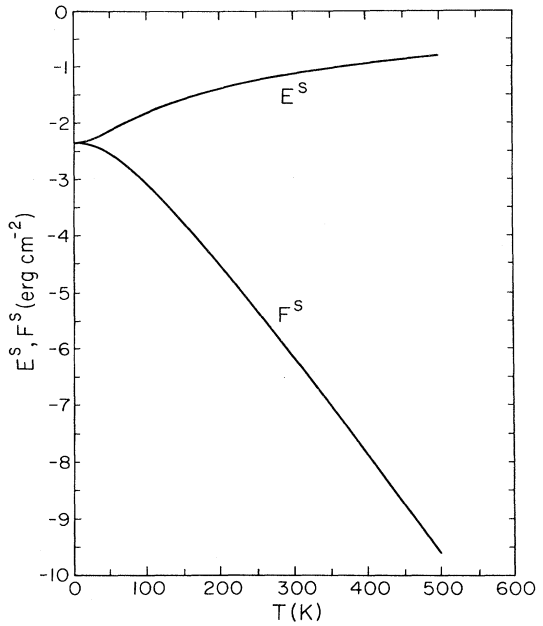

FIG. 8. Vibrational contributions to the surface thermodynamic functions E^S and F^S for the (0001) surface of graphite.

vector sampling grids. The results reported here were obtained for a 13-layer slab with a 12×12 Gaussian grid in the ISBZ, and a corresponding $12\times12\times12$ Gaussian grid in the irreducible part of the bulk BZ; for this slab thickness and at these grid densities the results have converged for all practical purposes.

In Fig. 8 we present E^S and F^S, and in Fig. 9, S^S and C_V^S for temperatures from $T=0$ up to 500 K. It is in-

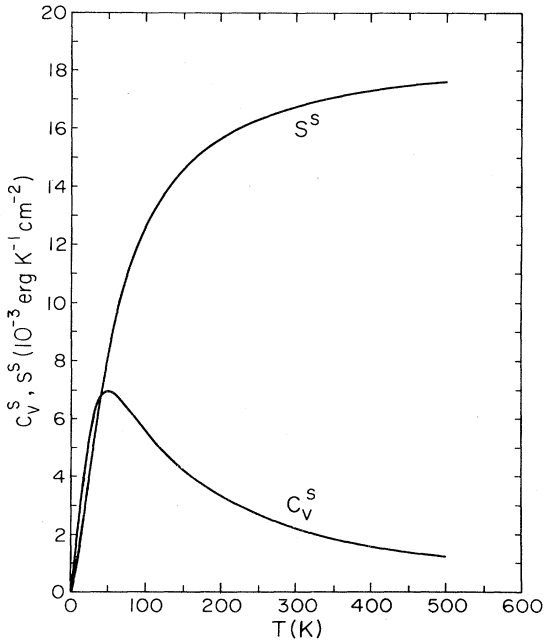

FIG. 9. Vibrational contributions to the surface thermodynamic functions S^S and C_V^S for the (0001) surface of graphite, as functions of temperature.

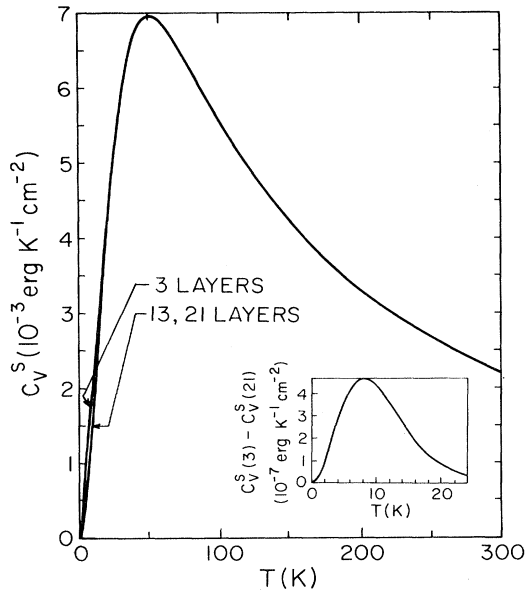

FIG. 10. Surface specific heat C_V^S for the 3-, 13-, and 21-layer graphite slabs, as functions of temperature. Inset: Difference C_V^S(3-layer slab)$-C_V^S$(21-layer slab) at low temperatures.

teresting to note that these quantities are roughly a factor of 10 smaller than the corresponding functions for the ionic crystals.[10] This is a result of the weak interplanar interactions in graphite, which diminishes the difference between a slab and the bulk: The creation of a surface is a much smaller perturbation than that in more isotropic crystals.

Of particular interest is the surface specific heat, because—among the four quantities—it is most directly amenable to experimental measurement. In Fig. 10 we compare the C_V^S results for 3-, 13-, and 21-layer slabs; the peak maximum lies at 50 K. Notice the small difference, at low T, between the 3-layer result, and the 13- and 21-layer results (the latter agreeing at all temperatures within the thickness of the line). This difference is attributable to the interaction of long-wavelength modes localized at opposite surfaces of the 3-layer slab, which gives rise to the lowering of some frequencies and hence a slight increase in C_V^S. The difference $C_V^S(3)-C_V^S(21)$ is plotted in the inset in Fig. 10; the curve has a shape typical of all excess specific-heat curves.

An interesting question that has been raised in connection with the specific heat of graphite is the excess linear temperature contribution at low temperatures, discussed by Van der Hoeven *et al.*,[23] which cannot be entirely attributed to electronic contributions. Fujita and Bugl[24] have attributed this excess linear contribution to the vibrations of finite lattices. These authors have pointed out that elastic plates exhibit a "flexural" mode with quadratic dispersion $[\omega(\bar{q}) \propto \bar{q}^2]$ at low frequencies, which leads to a linear temperature contribution to the specific heat, and they speculate that the excess linear temperature specific heat might be attributed to motions of this kind. We have looked for evidence of the flexural mode, both in the dynamics, by diagonalizing the dynamical matrix for very small wave vectors, as well as by attempting to fit the surface specific heat at very low temperatures by the expressions $\alpha T+\beta T^2$. In the dynamical results there is no evidence whatsoever of any frequency branch that is proportional to $\bar{q}^2$, and in fitting the specific-heat results the coefficient of the linear term α cannot be determined statistically. In their elastic calculations Fujita and Bugl find that a graphite plate 100 Å thick leads to a linear specific-heat contribution of about the correct magnitude. If such a contribution were significant in the lattice dynamics of graphite we should have found it for slabs of all three thicknesses.

The only measurements which we can compare to our results for the surface thermodynamic functions are those of de Sorbo and Nichols[3] for the specific heat. These authors measured the heat capacity of essentially bulk samples of Canadian natural graphite having layer thicknesses in excess of 900 Å in the [0001] direction, and of "graphitized lampblack" with a thickness of 110 Å. At 20 K (the highest temperature reported) the measured excess heat capacity of the lampblack graphite over the Canadian graphite (bulk) is of the order of 59×10^{-4} erg K^{-1} cm^{-2}. The calculated value at 20 K of 32×10^{-4} erg K^{-1} cm^{-2} is in surprisingly good agreement in light of the lack of definite characterization of the surface of the graphitized lampblack sample and its unknown defect state.

IV. FINAL COMMENTS

Of the two sets of quantities discussed in this paper—the MSA's and the thermodynamic quantities— the calculation of the MSA's requires particular care because of possible convergence difficulties. It should be emphasized that in this paper we are not interested in 2D systems; what we are studying is the behavior of the surface of 3D crystals of varying sizes. However, the methods at our disposal in slab calculations involve the use of systems with 2D periodicity. If one would try to compute the MSA's by fixing the thickness of the slab and successively refining the integration grid, one would be subject to the Landau-Peierls divergence effects.[13] But, for the present purpose these are artifacts of the calculational procedure and not relevant to the real finite-size and thermodynamic systems we wish to study. Consequently, we devised a different scheme of successive convergent approximations to avoid them. This scheme, involving parametrization of the crystals in terms of aspect ratio and thickness, is essential for going to the thermodynamic limit (vanishing surface-to-volume ratio) as a function of a *single* parame-

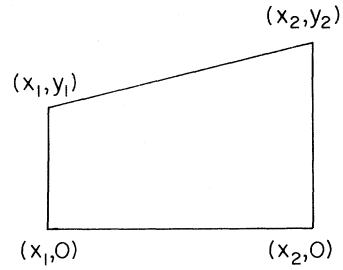

FIG. 11. Prototypical region for BZ integration.

ter (namely in inverse thickness), so that the extrapolation is practical.

The extrapolation procedure leads to shape independent results in the thermodynamic limit; a result which for surface MSA's was not *a priori* obvious to us, but which, *a posteriori,* is a valuable check on our convergence procedures. The central point is, that if one wishes to use slab calculations of MSA's to be relevant to large samples, an extrapolation procedure like ours is unavoidable—and at least for graphite the effect of extrapolation to the thermodynamic limit is large. We point out that this is the first time a procedure of this kind is used in practical calculations of surface MSA's.

ACKNOWLEDGMENT

Two of the authors (F.W. de W. and B. F.) acknowledge research support by the National Science Foundation under Grant No. DMR-81-21916 and by the Robert A. Welch Foundation.

APPENDIX: GAUSS-LEGENDRE QUADRATURE GRIDS

Consider R, the portion of BZ depicted in Fig. 11. We define variables ξ and η such as to map the region into the unit square in (ξ,η) space: Set

$$y=\eta\left[\xi+\frac{y_1}{y_2-y_1}\right](y_2-y_1)\ ,$$

$$x=\left[\xi+\frac{x_1}{x_2-x_1}\right](x_2-x_1)\ .$$

We thus have

$$\int_R dx\,dy\,f(x,y)=\int_0^1 d\xi\int_0^1 d\eta(x_2-x_1)(y_2-y_1)[\xi+y_1/(y_2-y_1)]f(x(\xi,\eta),y(\xi,\eta))\ .$$

We approximate the ξ and η integrals by Gauss-Legendre quadrature formulas: These are of the form

$$\int_0^1 du\phi(u)\simeq\sum_{1\le i\le n} w_i\phi(u_i)\ ,$$

where the u_i and w_i are tabulated quantities,[25] so

$$\int_R dx\,dy\,f(x,y)\simeq(x_2-x_1)(y_2-y_1)\sum_{1\le i\le n}\sum_{1\le j\le n} w_iw_j[u_i+y_1/(y_2-y_1)]f(x(u_i,u_j),y(u_i,u_j))\ .$$

*Present address: Shell Development Company, Bellaire Research Center, Houston, TX 77001.

[1]E. de Rouffignac, G. P. Alldredge, and F. W. de Wette, Phys. Rev. B 23, 4208 (1981).
[2]E. de Rouffignac, G. P. Alldredge, and F. W. de Wette, Phys. Rev. B 24, 6050 (1981).
[3]W. de Sorbo and G. E. Nichols, J. Phys. Chem. Solids 6, 352 (1958).
[4]B. J. C. van der Hoeven and P. M. Keesom, Phys. Rev. 130, 1318 (1963).
[5]P. Delhaes and Y. Hishiyama, Carbon 8, 31 (1970).
[6]G. H. Wostenholm and B. Yates, Philos. Mag. 27, 185 (1973).
[7]R. E. Allen and F. W. de Wette, Phys. Rev. 188, 1320 (1969).
[8]R. E. Allen and F. W. de Wette, Phys. Rev. 51, 4820 (1969).
[9]T. S. Chen, G. P. Alldredge, and F. W. de Wette, Surf. Sci. 57, 25 (1976).
[10]T. S. Chen, G. P. Alldredge, and F. W. de Wette, Surf. Sci. 62, 675 (1977); preliminary results were presented earlier by G. P. Alldredge, T. S. Chen, and F. W. de Wette, in *Low Temperature Physics—LT-13,* edited by K. D. Timmerhaus, W. J. O'Sullivan, and E. F. Hammel (Plenum, New York, 1974), Vol. 4, pp. 441–444.
[11]R. Nicklow, N. Wakabayashi, and H. G. Smith, Phys. Rev. B 5, 4951 (1972).
[12]G. P. Alldredge, E. de Rouffignac, B. Firey, and F. W. de Wette (unpublished).
[13]R. E. Peierls, Ann. Inst. Henri Poincaré 5, 177 (1935); L. D. Landau, Phys. Z. Sowjetunion 11, 26 (1937). A rigorous proof is given by N. D. Mermin, Phys. Rev. 176, 250 (1968). For a discussion of these divergence properties, see also Y. Imry, Ann. Phys. (N.Y.) 51, 1 (1969); Y. Imry and L. Gunther, Phys. Rev. B 3, 3939 (1971); P. Dutta and S. K. Sinha, Phys. Rev. Lett. 47, 50 (1981).
[14]Grafoil is the trade name of the pure graphite product distributed by Union Carbide Corporation.
[15]M. Nielson and J. P. McTague, Phys. Rev. B 19, 3096 (1979).
[16]H. C. Thacher, J. Chem. Phys. 32, 638 (1960).
[17]G. E. Bacon, Acta Crystallogr. 5, 492 (1952).
[18]R. Chen and P. Trucano, Acta Crystallogr. A 34, 979 (1978).
[19]J. G. Albinet, J. P. Biberian, and M. Bienfait, Phys. Rev. B 3, 2015 (1971).
[20]J. P. Biberian, M. Bienfait, and J. B. Theeten, Acta Crystallogr. A 29, 221 (1973).
[21]G. Boata, P. Cantini, C. Salvo, R. Tatarek, and S. Terreni, Surf. Sci. 114, 485 (1982).
[22]Cf., e.g., T. H. K. Barron, and M. L. Klein, Proc. Phys. Soc. London 85, 533 (1965).
[23]B. J. C. Van der Hoeven, Jr., P. M. Keesom, J. W. McClure, and G. Wagoner, Phys. Rev. 152, 796 (1966).
[24]S. Fujita and P. Bugl, Phys. Rev. 185, 1094 (1969).
[25]M. Abramowitz and I. A. Stegun, *Handbook of Mathematical Functions,* U. S. Nat. Bur. Stand. (Appl. Math. Ser. No. 55), edited by M. Abramowitz and I. A. Stegun (U. S. G.P.O., Washington, D.C., 1964), p. 917.